Lehmann rotation of twisted bipolar cholesteric droplets: role of Leslie, Akopyan and Zel'dovich thermomechanical coupling terms of nematodynamics

P. Oswald, G. Poy & A. Dequidt

 View supplementary material

 Published online: 28 Nov 2016.

 Submit your article to this journal

 View related articles

 View Crossmark data

Lehmann rotation of twisted bipolar cholesteric droplets: role of Leslie, Akopyan and Zel'dovich thermomechanical coupling terms of nematodynamics

P. Oswald[a], G. Poy[a] and A. Dequidt[b,c]

[a]Laboratoire de Physique, Univ Lyon, Ens de Lyon, Univ Claude Bernard, CNRS, Lyon, France; [b]Institut de Chimie de Clermont-Ferrand, Université Clermont Auvergne, Université Blaise Pascal, Clermont-Ferrand, France; [c]CNRS, UMR 6296, ICCF, Aubière, France

ABSTRACT

We show that the Leslie and texture-dependent Akopyan and Zel'dovich thermomechanical coupling terms of nematodynamics cannot explain the thermal Lehmann rotation of the twisted bipolar droplets observed in the coexistence region between a cholesteric phase and the isotropic liquid. On the other hand, these terms are pertinent below the transition temperature and can be determined by measuring the director rotation velocity in two different molecular configurations. In addition, a complete characterisation of the liquid crystal used (CCN-37) is also given.
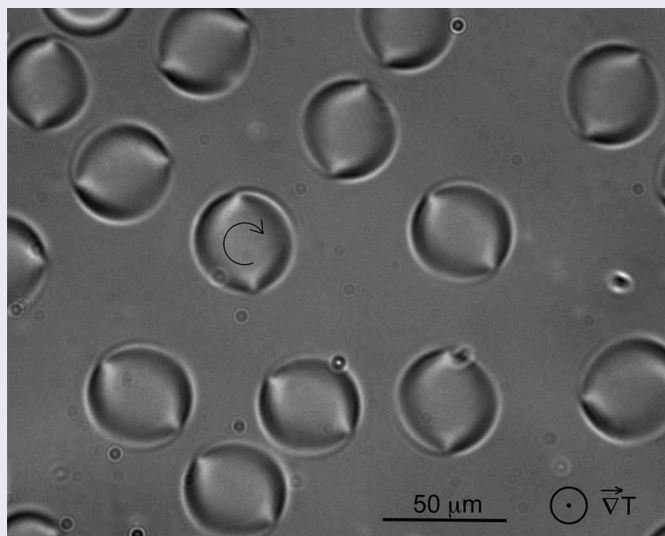
1. Introduction

A cholesteric phase is a nematic phase twisted in a single direction of the space [1]. It is characterised by the cholesteric pitch P which is the distance over which the director $\vec{n}$ rotates by 2π. The cholesteric-to-isotropic phase transition being first order, it is possible to observe cholesteric droplets in coexistence with the isotropic liquid. In 1900, Otto Lehmann observed that the internal texture of the droplets rotates constantly when a temperature gradient is applied, a phenomenon known as the Lehmann effect [2]. This thermomechanical effect, which was reobserved recently in cholesteric liquid crystals (LCs) [3–6], was shown to also exist in a *nematic* chromonic LC featuring twisted bipolar droplets [7]. This observation is surprising because it was so far accepted that the Lehmann effect could only be observed in a chiral phase (made of chiral molecules in the case of a cholesteric phase). This result is important because it shows that the Lehmann rotation is due to the macroscopic twist of the director field inside the droplets and not directly to the chirality of the phase. Note that in the experiments with the chromonic LC the director field is twisted at equilibrium because of the giant elastic anisotropy of

---

the phase, the twist constant K_2 being orders of magnitude smaller than the splay and bend constants K_1 and K_3 [8]. In addition, the director field inside the droplets can be indifferently twisted to the right or to the left because the nematic phase is not chiral. For this reason, the same proportion of droplets rotating clockwise and counterclockwise was observed.

In order to explain the Lehmann rotation of the twisted bipolar droplets in the chromonic nematic phase, we used a model similar to the Leslie model based on the existence in a distorted nematic phase of a thermomechanical torque proportional to the temperature gradient. This texture-dependent torque was first given by Akopyan and Zel'dovich [9] and was recalculated more rigorously by Pleiner and Brand [10]. It reads [11]

$$\vec{\Gamma}_{TM} = \vec{n} \times \vec{f}_{TM}, \tag{1}$$

where $\vec{f}_{TM}$ is a thermomechanical force of general expression:

$$\begin{aligned}
\vec{f}_{TM} = &\ \bar{\xi}_1 (\vec{\nabla} \cdot \vec{n}) \vec{G} + \bar{\xi}_2 (\vec{n} \cdot \vec{\nabla} \times \vec{n})(\vec{n} \times \vec{G}) \\
&+ \bar{\xi}_3 (\vec{n} \cdot \vec{G})\big((\vec{\nabla} \times \vec{n}) \times \vec{n}\big) \\
&- \bar{\xi}_4 \vec{\nabla} \cdot (\vec{G} \otimes \vec{n} - \vec{G} \cdot \vec{n} \mathbb{I}).
\end{aligned} \tag{2}$$

In this form, the splay, twist and bend contributions to the director field distortions are easily recognisable. Note that $\mathbb{I}$ is the identity matrix and $\otimes$ denotes the dyadic product of two vectors (with $(\vec{a} \otimes \vec{b})_{ij} = a_i b_j$) and the $\bar{\xi}_i$ are linear combinations of the original Akopyan and Zel'dovich ξ_i coefficients or Pleiner and Brand Π_i coefficients.[1] This formula considerably simplifies (up to an additive term proportional to $\vec{n}$ which gives a zero contribution to the thermomechanical torque) under the assumption, which we will use here, that all the $\bar{\xi}_i$ are equal to $\bar{\xi}$:

$$\vec{f}_{TM} = \bar{\xi} \left(\vec{G} \cdot \vec{\nabla} \right) \vec{n}. \tag{3}$$

This model allowed us to explain the observations and led to a value of 80 pN K^{-1} for the constant $\bar{\xi}$. This value is surprisingly large in comparison with the value of 10 fN K^{-1} given by Akopyan and Zel'dovich in their paper [9].

The aim of this paper is to test the validity of this model for the bipolar droplets by measuring separately the average constant $\bar{\xi}$ by using a more direct and reliable method. As we have shown recently [11], this is theoretically possible by measuring the rotation velocity of the director in the cholesteric phase in two different geometries, below the transition temperature. This method requires us to prepare well-oriented

samples with surfaces treated for tangential sliding or homeotropic anchoring.

Unfortunately, we do not know how to achieve homeotropic anchoring with the chromonic LC. For this reason, we used instead a thermotropic LC for which adequate surface treatments are available. We also chose a LC that gives a tangential anchoring at the nematic–isotropic interface. This is essential to obtain bipolar droplets in the coexistence region with the isotropic liquid. On the other hand, we did not find a thermotropic LC in which the constant K_2 is much smaller than K_1 and K_3. For this reason, the bipolar droplets do not spontaneously twist in the nematic phase and the only way to obtain twisted bipolar droplets is to dope the LC with a small amount of a chiral impurity.

The paper is structured as follows. In Section 2, we recall the theoretical background of the generalised thermomechanical model and give the formulas for the rotation velocity of the textures. In Section 3, we present the materials and methods used experimentally. In Section 4, we show our experimental results obtained below the phase transition with two different textures and give the experimental values of the Leslie and Akopyan and Zel'dovich thermomechanical constants. Section 5 is devoted to the twisted bipolar droplets with special emphasis on the thickness effects and the flow detection by photobleaching around the droplets. Our conclusions on the role in the Lehmann effect of the thermomechanical coupling terms of Leslie, Akopyan and Zel'dovich are drawn in Section 5.

2. A survey of previous theoretical results

We recalled in the introduction that the director experiences a torque when the LC is subjected to a temperature gradient $\vec{G}$. In a cholesteric phase, this torque reads

$$\vec{\Gamma}_{TM} = \vec{n} \times (\nu \vec{n} \times \vec{G} + \vec{f}_{TM}), \tag{4}$$

where the force $\vec{f}_{TM}$ is given in Equation (2). The coefficient ν is the well-known thermomechanical Leslie coefficient [12]. This term vanishes in a nematic phase by symmetry. The other contribution in $\vec{n} \times \vec{f}_{TM}$ contains the texture-dependent terms [9,10] and exists both in nematic and cholesteric LCs. All these terms may lead to a continuous rotation of the director and, thus, of the texture observed in the microscope. Nevertheless, two conditions are required to observe a rotation: the total free energy of the system must remain constant in time and the director must be free to rotate azimuthally at the surfaces limiting the

cholesteric domain. In the following, we will assume that all the $\bar{\xi_i}$'s are equal by using the simplified expression (3) of $\vec{f}_{TM}$ and we will neglect the surface dissipation.

The translationally invariant configurations (TICs) provide the simplest examples of rotating textures. In practice, they develop below the transition temperature, when the cholesteric phase is confined between two parallel glass plates. The temperature gradient is applied along the normal to the plates (z-axis). The texture of a TIC depends on the anchoring conditions on the glass. Two types of anchoring can be used, the tangential sliding anchoring and the homeotropic one.

When the two plates are treated for tangential sliding anchoring, the rotation velocity of the director in the linear regime (small G) reads [11]

$$\omega_p = -\hat{G} \frac{\kappa_g}{\kappa_\perp} \frac{\bar{v}}{\gamma_1}, \tag{5}$$

where $\bar{v} = v - \bar{\xi} q_0$ is the thermomechanical coefficient measured in this geometry – and that we actually measured in all of our previous experiments [3,13]. In this expression, $q_0 = \frac{2\pi}{P}$ is the equilibrium twist, $\hat{G} = \frac{\Delta T}{4e}$ is the imposed temperature gradient by denoting by e the thickness of the glass plates (2 for the sample + 1 in each oven see Figure A5 in the Appendix) and by ΔT the temperature difference between the top and bottom ovens, κ_g is the thermal conductivity of the glass, $\kappa_\perp$ is the thermal conductivity of the LC perpendicular to the director and γ_1 is the rotational viscosity. Note that the actual temperature gradient inside the LC is $G = \hat{G} \frac{\kappa_g}{\kappa_\perp}$.

When one plate is treated for homeotropic anchoring and the other for tangential sliding anchoring (mixed anchoring), the rotation velocity becomes [11]

$$\omega_m = -\hat{G} \frac{\kappa_g}{\kappa_\parallel} \frac{\bar{v} I_v + \bar{\xi} q_0 I_\xi}{\gamma_1 I_\gamma}, \tag{6}$$

where the dimensionless integrals are defined as

$$I_v = \frac{1}{d} \int_0^d \frac{\sin^2 \alpha}{1 - \epsilon \sin^2 \alpha} \, dz, \tag{7}$$

$$I_\xi = \frac{1}{q_0 d} \int_0^d \frac{(q_0 - \phi_{,z}) \sin^2 \alpha}{1 - \epsilon \sin^2 \alpha} \, dz, \tag{8}$$

$$I_\gamma = \frac{1}{d} \int_0^d \sin^2 \alpha \, dz. \tag{9}$$

Here, the bottom (top) surface is at $z = 0$ ($z = d$) and $\epsilon = 1 - \kappa_\perp / \kappa_\parallel$ is the relative anisotropy of thermal conductivity, by denoting by $\kappa_\perp$ ($\kappa_\parallel$) the LC thermal conductivity perpendicular (parallel) to the director. The director components are

$$\vec{n}_0 = \begin{pmatrix} \sin \alpha \cos \phi \\ \sin \alpha \sin \phi \\ \cos \alpha \end{pmatrix}, \tag{10}$$

where angles α and ϕ only depend on z (with the z-axis oriented upwards). These integrals can be calculated numerically with Mathematica once the two differential equations $\frac{\delta f}{\delta \alpha} = 0$ and $\frac{\delta f}{\delta \phi} = 0$ (where f is the Frank elastic energy [1]) that give α and ϕ are solved. This requires us to know the elastic constants K_1, K_2 and K_3 (see Appendix).

These results show that measuring ω_p and ω_m allows us to calculate $\bar{v}$ and $\bar{\xi}$ by using the following formulas:

$$\frac{\bar{v}}{\gamma_1} = -\frac{\omega_p}{\hat{G}} \frac{\kappa_\perp}{\kappa_g}, \tag{11}$$

$$\frac{\bar{\xi} q_0}{\gamma_1} = \frac{\omega_p}{\hat{G}} \frac{\kappa_\perp}{\kappa_g} \frac{I_v}{I_\xi} - \frac{\omega_m}{\hat{G}} \frac{\kappa_\parallel}{\kappa_g} \frac{I_\gamma}{I_\xi}. \tag{12}$$

For the Lehmann droplets, the calculation shows that the thermomechanical coupling terms leads to a rotation at velocity [7,11]:

$$\omega = G \frac{\bar{v} L_v + \bar{\xi} q_0 L_\xi}{\gamma_1 L_\gamma}, \tag{13}$$

where the dimensionless integrals L_γ, L_v and L_ξ are defined as

$$L_\gamma = \frac{1}{V} \int_V \left(\frac{D\vec{n}_0}{D\Phi} \right)^2 dV, \tag{14}$$

$$L_v = \frac{1}{V} \int_V (\vec{n}_0 \times \vec{e}_z) \cdot \frac{D\vec{n}_0}{D\Phi} \, dV, \tag{15}$$

$$L_\xi = \frac{1}{q_0 V} \int_V \left[\left(\vec{e}_z \cdot \vec{\nabla} \right) \vec{n}_0 - q_0 \vec{e}_z \times \vec{n}_0 \right] \cdot \frac{D\vec{n}_0}{D\Phi} \, dV. \tag{16}$$

Here, Φ represents the angle of rotation of the internal texture of the droplets. It can be shown that $\frac{D\vec{n}_0}{D\Phi} = \vec{e}_z \times \vec{n}_0 - \frac{\partial \vec{n}_0}{\partial \vartheta}$ [3] by denoting by ϑ the polar angle in cylindrical coordinates and by $\vec{e}_z$ the unit vector in the z-direction. These integrals can be calculated numerically providing that the director field inside the droplets is known. We recall that this formula was obtained by assuming that there is no flow (as observed experimentally, see Section 4 and Ref. [14]), and the temperature gradient inside the droplets is constant, given by $G = \hat{G} \frac{\kappa_g}{\bar{\kappa}}$ where $\bar{\kappa}$ is an average heat conductivity of the LC of the order of $\frac{\kappa_\parallel + 2\kappa_\perp}{3}$.

3. Materials and methods

The LC chosen is CCN-37 (or $4\alpha,4'\alpha$-propylheptyl-$1\alpha,1'\alpha$-bicyclohexyl-4β-carbonitrile from Nematel, Germany). This LC has a nematic phase of negative dielectric anisotropy and very small birefringence [15] between 22.5°C and 54.1°C. More interesting – and rather rare – the anchoring is tangential at the nematic–isotropic interface, as confirmed by dielectric measurements (see Appendix). For this reason, the nematic droplets observed in the coexistence region with the isotropic liquid have a bipolar texture. The droplets are not spontaneously twisted because the twist constant K_2 is comparable with the splay and bend constants K_1 and K_3 (see Appendix and Table 1 in which the values of the material constants at the transition temperature are given). This is expected from the theory [16]. For this reason, the nematic droplets of pure CCN37 do not rotate under the temperature gradient [7]. To twist the director field inside the droplets and observe the Lehmann rotation, the nematic phase was made cholesteric by doping the CCN37 with a small amount of CC (cholesteryl chloride from Sigma-Aldrich, Germany) or R811 (R-(+)-octan-2-yl 4-((4-(hexyloxy)benzoyl)oxy) benzoate from Merck, Germany). The helical twist power (HTP; defined as HTP = $1/(PC)$, where P is the cholesteric pitch and C is the mass fraction of chiral dopant) of these two chiral dopants is very different as can be seen in Appendix and Table 1.

The samples were prepared between two parallel glass plates, and nickel wires of calibrated diameter were used as a spacer. The sample thickness was systematically measured before filling with a spectrometer. All the samples with more than three interference fringes over the whole surface area were systematically rejected. The sliding tangential anchoring was obtained by spin-coating at 800 rpm for 15 s a thin layer of a polymercaptan (hardener of the epoxy glue Structuralit7 from Eleco) dissolved in 2-butanone with a concentration of 5% by weight. The polymercaptan layer was then baked at 60°C during 10 min under vacuum (0.1 Pa) to evaporate the solvent. After baking, the polymercaptan layer is 200 nm thick [17]. It must be noted that the polymercaptan is very little soluble in the CCN37. This could explain why the anchoring remains perfectly sliding during several days even when the director does not rotate. This absence of memorisation of the anchoring direction (contrary to what is observed with usual nematic materials [17]) is remarkable and made easier the measurements of the thermomechanical coefficients. Polyimide Nissan 0626 was used to achieve strong homeotropic anchoring. It was dissolved in solvent 26 from Nissan (3% by weight) and deposited by spin-coating at 3000 rpm for 90 s. The layer was then dried for 1 min at 80°C and baked at 180°C for 30 min. Polyimide Nissan 0825 was used to achieve planar anchoring. It was dissolved in solvent 25 from Nissan (5% by weight) and deposited by spin-coating at 3000 rpm for 90 s. The layer was then dried for 1 min at 80°C and baked at 280°C for 30 min. Unidirectional anchoring was obtained by rubbing the surface with a felt cloth. All the samples were filled by capillarity and sealed on the sides with UV glue NOA 81 (Norland Optical adhesive). The ovens used to impose a temperature gradient and the fluorescence recovery after photobleaching (FRAP) set-up used to detect a possible flow around the droplets are described in Refs. [3] and [14], respectively. In the following, we shall need the values of the elastic constants, the rotational viscosity, the thermal conductivities and the HTP of the chiral dopants. The values of these constants at the transition temperature are given in Table 1. To obtain these constants, we need to measure additional quantities such as the dielectric constants and the birefringence. The details of these measurements are given in Appendix. Note that for completeness we measured these constants in a large range of temperature, with a special emphasis on their pretransitional behaviour and their values at the transition temperature.

4. Experimental determination of the constants ν and $\bar{\xi}$ from the TICs rotation

In Section 2, we have seen that measuring the rotation velocity of the director in two TICs with different orientations allows the determination of both the Leslie coefficient ν and the nematic-like thermomechanical constant $\bar{\xi}$ (assuming that all the $\bar{\xi}_i$ are equal). We performed these measurements with two cholesteric mixtures CCN-37 + 3 wt% CC and CCN-37 + 0.166% R811. The concentrations of CC and R811 were chosen in order that the equilibrium twist is the same in the two mixtures at the transition temperature, namely $q_0 \approx 10^5 \mathrm{m}^{-1}$ which corresponds to a cholesteric pitch $P \approx 60$ μm (Appendix). The rotation velocity of the

Table 1. Values at the transition temperature of the main physical constants of CCN-37.

| Constants	K_1 (pN)	K_2 (pN)	K_3 (pN)	$\frac{\kappa_g}{\kappa_\parallel}$	$\frac{\kappa_g}{\kappa_\perp}$	γ_1 (Pa s)	HTP$_{CC}$ (μm^{-1})	HTPR811 (μm^{-1})
Values at T_{Chl}	0.96	0.84	1.37	5.1	7.4	0.0069	0.56	9.3

director is measured by recording the transmitted intensity between crossed polarisers in a region where the director rotates regularly.

In samples treated for tangential sliding anchoring on both surfaces (simply called planar sliding samples in the following), $\pm 1/2$ disclination lines are usually observed. Figure 1 shows a $-1/2$ defect in a sample of thickness 10.6 μm and a recording of the transmitted intensity when a temperature difference $\Delta T = 40°C$ is imposed. The corresponding video S1 is shown in the supplemental material. Let Θ be the period of the optical signal. Because the intensity passes through a minimum each time the director rotates by $\pi/2$, the angular rotation velocity of the director is given in absolute value by $|\omega| = \pi/(2\Theta)$. The sign of ω is given by observing the sense of rotation of the extinction branches of the defects, knowing that the molecules rotate in the same direction as the branches of the negative defects [18]. For instance, in Figure 1, the branches of the $-1/2$ defect rotate clockwise, meaning that $\omega < 0$ when $G > 0$ by taking the z axis pointing towards the reader.

In samples with the bottom surface treated for homeotropic anchoring and the upper surface treated for sliding tangential anchoring (called mixed sample in the following), the texture remains stable with respect to the formation of periodic cholesteric fingers on the condition that the confinement ratio $C = d/P$ is smaller than typically 0.5

[19]. This condition is fulfilled in all of our experiments in which $C<0.2$. Because of the mixed anchoring, the only possible defects are ± 1 defects as can be seen in Figure 2(a). In this case, the period must be measured far from the ± 1 defect because its branches rotate irregularly in its immediate vicinity as can be seen in the video S2 of the supplemental material. This effect is due to the elastic anisotropy of the cholesteric phase – the circular configuration of a $+1$ defect costing more elastic energy than its radial configuration since $K_3 > K_1$ (Appendix). The intensity measured at $\Delta T = 40°C$ close to the -1 defect where the rotation is regular is shown in Figure 2(b).

Finally, the rotation velocity ω measured in the planar sliding and mixed samples as a function of the average temperature of the sample is shown in Figure 3 for the mixture CCN-37 +3% CC when $\Delta T = 40°C$. This graph shows that, for the same imposed ΔT, the texture rotates more slowly in mixed samples than in planar sliding samples whatever the temperature. For instance, we measured at the transition temperature $\omega = \omega_p^{CC} \approx -0.0125$ rad/s in the planar sliding samples and $\omega = \omega_m^{CC} \approx -0.00714$ rad/s in the mixed samples. The rotation velocity also decreases in all samples when the temperature decreases. This effect is mainly due to the increase of the rotational viscosity γ_1 when the temperature decreases (Appendix) [13].
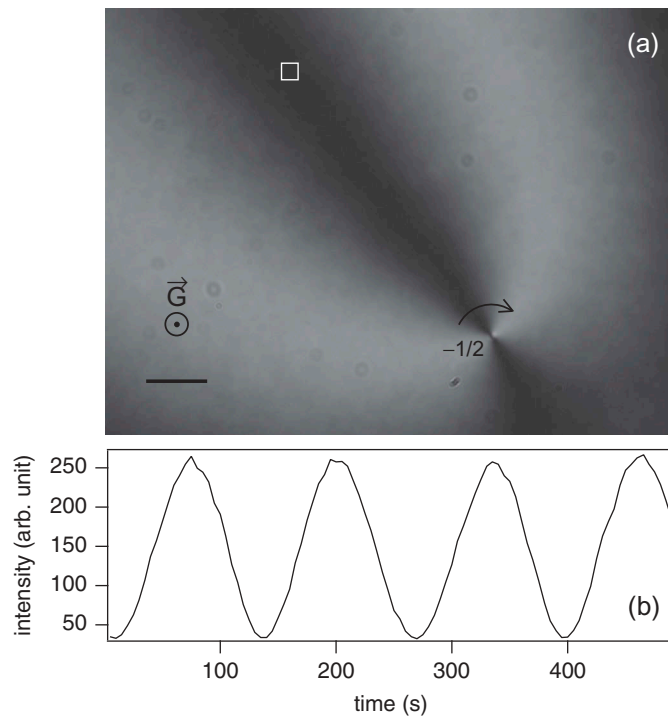
Figure 1. (a) $-1/2$ disclination line observed between crossed polarisers just below the transition temperature ($\delta T = T - T_{Chl} \approx -0.05°C$, by denoting by T the LC temperature at the interface with the hot glass plate and by T_{Chl} the solidus temperature) in a planar sliding sample of the mixture CCN-37 +3%CC. $d = 10.6$ μm and $\Delta T = 40°C$. The bar represents 50 μm. (b) Intensity recorded inside the white square shown in the photo as a function of time.
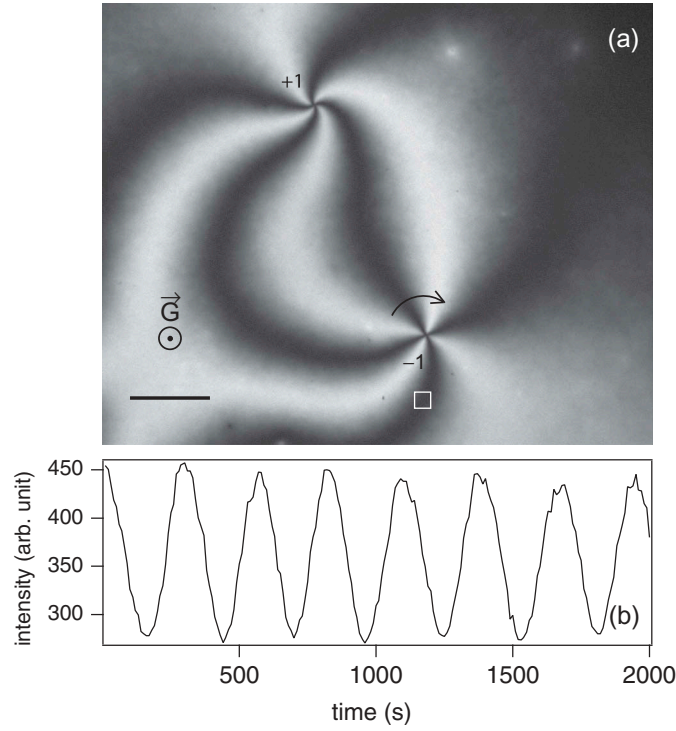
Figure 2. (a) Pair of ± 1 disclination lines observed between crossed polarisers just below the transition temperature ($\delta T \approx -0.05°C$ in a mixed sample of the mixture CCN-37 +3%CC. $d = 10.8\ \mu m$ and $\Delta T = 40°C$. The bar represents 100 μm. (b) Intensity recorded inside the white square shown in the photo as a function of time.
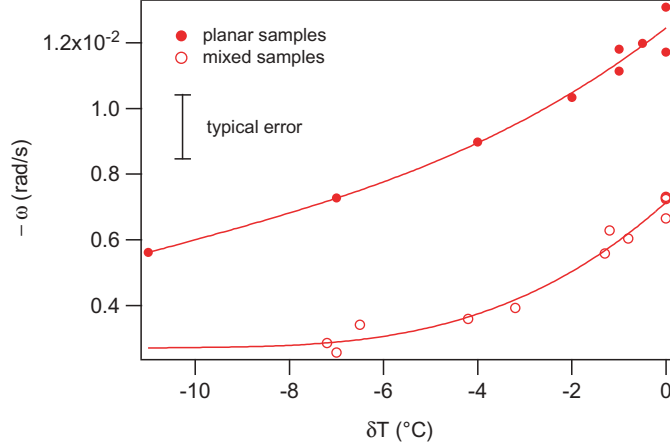
Figure 3. (Colour online) Angular rotation velocity ω as a function of the temperature difference δT when $\Delta T = 40°C$. Mixture CCN-37 +3% CC. Note that ω is negative (for a positive temperature gradient) in planar sliding and mixed samples.

From these data, we calculated ν and $\bar{\xi}$ at the transition temperature T_{ChI} at which we measured the conductivity ratios $\kappa_\parallel/\kappa_g$ and $\kappa_\perp/\kappa_g$ (see Appendix and Table 1). With the values of the elastic constants given in Table 1, we solved numerically the differential equations $\frac{\delta f}{\delta \alpha} = 0$ and $\frac{\delta f}{\delta \phi} = 0$ given $\alpha(z)$ and $\theta(z)$ in the mixed samples and calculated numerically the integrals given in Equations (7)–(9): $I_\nu = 0.66$, $I_\xi = 0.59$ and $I_\gamma = 0.50$. From these values and the values of the material constants given in Table 1 we found, by using Equations (11) and (12), $\bar{\nu}(CC) = 1.13 \pm 0.1\ 10^{-9}\ Nm^{-1}\ K^{-1}$ and $\bar{\xi} = -0.44 \pm 0.23\ 10^{-14}\ NK^{-1}$, or equivalently knowing that $q_0 = 10^5 m^{-1}$:

$$\bar{\nu}/q_0(CC) = 11.3 \pm 1\ fNK^{-1},$$
$$\bar{\xi} = -4.4 \pm 2.3\ fNK^{-1},$$

where the error bars have been calculated by taking into account only the errors on ω_p and ω_m. This value

of $\bar{v}/q_0$ is comparable to that obtained with other diluted cholesteric mixtures [13].

For completeness, we performed similar measurements with a second mixture CCN-37 +0.166% R811 at the transition temperature. With this mixture, we found in the planar sliding samples $\omega_p^{R811} = -0.0032$ rad/s. In the mixed samples, the rotation velocity was impossible to measure in spite of repeated attempts, suggesting that $\omega_m^{R811} \sim 0$ rad/s. Because q_0 is the same as in the previous mixture, the integrals I_v, I_ξ and I_γ remain unchanged. From Equations (11) and (12), we calculate at the transition temperature $\bar{v}(R811) = 0.3 \pm 0.09\ 10^{-9}$N m^{-1}K^{-1} and $\bar{\xi} = -0.32 \pm 0.23\ 10^{-14}$N K^{-1}, or equivalently knowing that $q_0 = 10^5$m^{-1}:

$$\bar{v}/q_0(R811) = 3 \pm 0.9\ \text{fNK}^{-1}$$
$$\bar{\xi} = -3.2 \pm 2.3\ \text{fNK}^{-1}.$$

These measurements show that the value of the measured Leslie coefficient $\bar{v}$ (or of the ratio $\bar{v}/q_0$) depends on the chiral molecules, whereas the value of $\bar{\xi}$ is the same for the two mixtures within the experimental errors. This is expected because $\bar{\xi}$ is a nematic-like thermomechanical coefficient that should essentially depend on the LC used, here the CCN-37. It must be emphasised that $\bar{v}$ is only 3.8 times smaller in the mixture with R811 than in the mixture with the CC, although the concentration of R811 is 18 times smaller than that of CC. This means that the Leslie effect is 18/3.8 = 4.7 times stronger with the R811 than with the CC at equal concentrations. In other words, the Leslie rotatory power (defined to be LRP $=\bar{v}/(2\pi C)$ in Ref. [13]) of the R811 is 4.7 times larger than the LRP of the CC, although the HTP of the R811 is 18 times larger than that of the CC. This shows that the HTP and the LRP have not the same origin, the former corresponding to an equilibrium property whereas the second one is dynamic in nature.

Another point to mention here is that our velocity measurements are compatible with the anisotropic thermomechanical model in which the constants $\bar{\xi}_i$ are all different. Indeed, Equation (5) remains unchanged in the general case (on condition to take $\bar{v} = v - \bar{\xi}_2 q_0$) while, in Equation (6), the term $\bar{\xi} q_0 I_\xi$ must be replaced by a sum $\sum_1^4 \bar{\xi}_i q_0 I_i$ where the dimensionless integrals I_i only depend on the director field $\vec{n}_0$. If q_0 is the same in all the samples (here, $q_0 = 10^5$m^{-1}), these formulas show that one must have

$$\delta\omega^{CC} = \delta\omega^{R811}, \tag{17}$$

by setting $\delta\omega = \omega_m - \frac{\kappa_\perp}{\kappa_\parallel} \frac{I_v}{I_\gamma} \omega_p$. To test this relation, we calculated $\delta\omega^{CC}$ and $\delta\omega^{R811}$ with the values of the

rotation velocities given above. This gives $\delta\omega^{CC} = 0.0037 \pm 0.0024$ rad/s and $\delta\omega^{R811} = 0.0028 \pm 0.0019$ rad/s. As expected, these two values are equal to each other to within the experimental errors, confirming that the Akopyan and Zel'dovich terms are well responsible for the velocity difference measured between planar sliding and mixed samples of the same mixture.

Another remarkable fact is that the value of $\bar{\xi}$ is almost four orders of magnitude smaller than that measured in the chromonic nematic LC from the Lehmann rotation of the twisted bipolar droplets ($\bar{\xi} \approx 80$ pN K^{-1} [7]). A priori $\bar{\xi}$ must be of the same order of magnitude in all the LCs. This result suggests that the Lehmann rotation observed in the chromonic LC is not due to the thermomechanical coupling of Akopyan and Zel'dovich. In order to confirm this point, we measured the rotation velocity of the twisted bipolar droplets in the mixtures CCN-37+CC and CCN-37+R811 used in this study.

5. Experimental determination of the constants v and $\bar{\xi}$ from the droplets rotation

We have shown in Appendix that the anchoring is tangential at the nematic–isotropic interface of the CCN-37 LC. From a theoretical point of view, this anchoring must favour the formation of bipolar nematic droplets in the region of coexistence with the isotropic liquid [16]. This is indeed what we observed experimentally under the microscope. We also observed that the droplets do not rotate when a temperature gradient is imposed, which clearly indicates that they are not twisted in the nematic phase. This is expected because the twist constant is of the same order of magnitude as the bend and splay constants in CCN-37 (Appendix and Table 1). To twist the director field inside the droplets, we doped the LC with small amounts of CC or R811. With these cholesteric mixtures, we observed that all the droplets oriented with the bipole axis perpendicular to the temperature gradient were rotating in the same direction (Figure 4 and video S3 of the supplemental material). In addition, ω and G were of opposite sign in all mixtures.

Before quantitatively studying this rotation, we tracked the presence of a flow inside the droplets by using the photobleaching experiment described in Ref. [14]. This point is important because our model assumes that the texture – and not the droplet itself – rotates, implying that there is no flow. The experiment was performed with a 21-μm-thick sample of the mixture CCN-37 +5.9 wt% CC
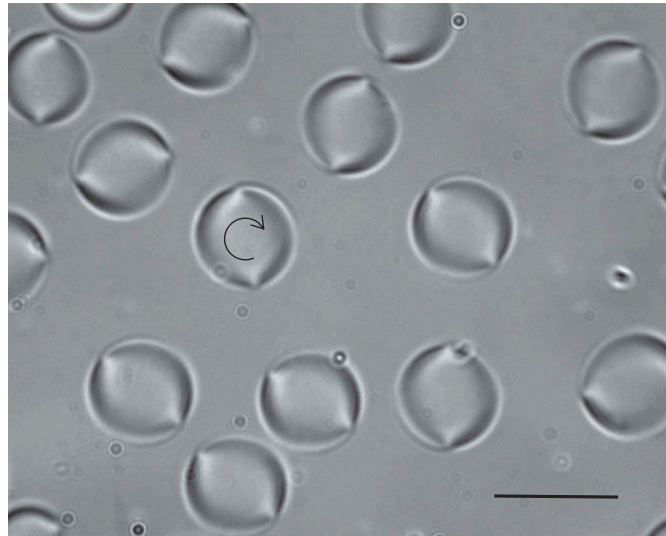
Figure 4. Bright field microscopy images of twisted bipolar droplets in a sample of CCN-37 +5.9%CC. They all rotate clockwise as can be seen in the video S3 of the supplemental material. The bar represents 50 μm. $\Delta T = 1.25°$C and $d = 50$ μm.

doped with 0.05 wt% of the fluorescent dye NBD C6-ceramide ((N-[2-hydroxy-1-(hydroxymethyl)-3-heptade-cenyl]-6-[(7-nitro-2,1,3-benzoxadiazol-4-yl)amino], Interchim, France). To limit the heating effects and avoid that the droplet melts during the laser shot, the sample was sandwiched between two 1-mm-thick sapphire plates treated for tangential sliding anchoring. With these plates, the temperature gradient inside the sample is about twice as large – for the same ΔT – as with ordinary glass plates. Figure 5 shows the example of a shot on the outer side of a droplet of radius 35 μm and the results of

the fit with the Gaussian function $s_0(t) + \Delta s(t) \exp\left\{-\frac{[x-x_0(t)]}{2\sigma(t)^2}\right\}$ of the fluorescence signal $\hat{s}(x, t)$ corrected for the non-uniformity of the lighting and for the natural photobleaching of the dye during the acquisition (for details, see Ref. [14]). This example shows that the centre of the bleached spot (marked with a white dot in the top images of Figure 5) does not move during the rotation of the droplet within the experimental noise (see also video S4 of the supplemental material). This indicates that there is no visible flow in the plane of the
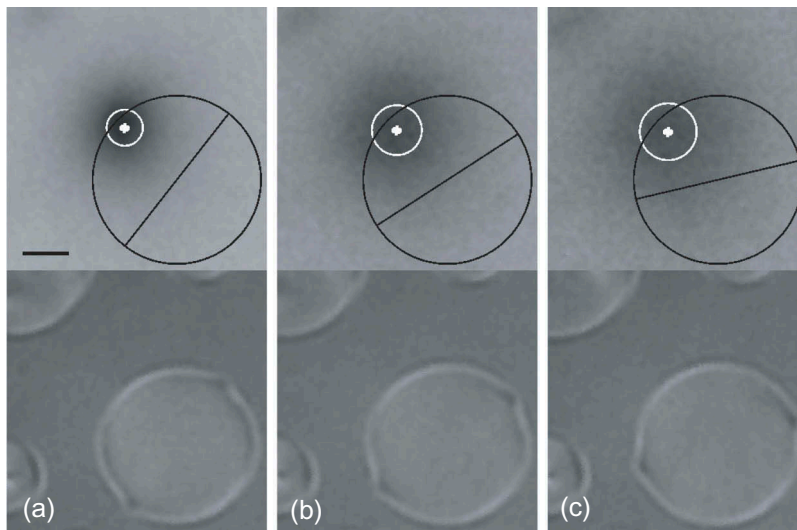
Figure 5. Fluorescence signal after photobleaching (top images) and images in reflexion between crossed polarisers of the droplet under white light illumination (bottom images) at times $t = 0.5$s (a), $t = 10.17$s (b) and $t = 19.84$s. The horizontal black bar represents 10 μm. The black circle represents the outer contour of the droplet. The tilted black line gives the orientation of the bipole. The white dot represents the centre $x_0(t)$ of the fitted Gaussian function, and the white circle represents the circle of equation $x - x_0(t) = \sigma/2$. In this experiment, $\Delta T = 2.5°$C. Sample of CCN-37 +5.9% CC, $d =$21 μm.

sample and that the droplet does not rotate as a rigid body. The same conclusion was already reached for the banded droplets observed in usual cholesteric mixtures [14]. Note that we fitted the whole spot in this experiment. This was possible because the droplet is almost invisible in fluorescence microscopy, the optical indices of the isotropic liquid and of the nematic phase being almost equal in the coexistence region where the birefringence is of the order of 0.0165 (Appendix). Note also that the spot remains circular in time to a very good approximation. This comes from the fact that the director orientation changes within the bleached spot and that the average diffusion coefficient of the dye in the nematic phase $(D_\parallel + 2D_\perp)/3$ is very close to the diffusion coefficient of the dye in the isotropic liquid D_I (Appendix).

To study quantitatively the rotation, we prepared mixtures of CCN-37+CC and CCN37+R811 and systematically measured the period of rotation Θ of the droplets as a function of their radius R for different ΔT and concentrations of chiral dopants. In these experiments, all the samples were treated for tangential sliding anchoring on the two plates and only the droplets with the bipole parallel to the glass plates were measured.

Figure 4 shows several droplets rotating in the same direction under the action of a temperature gradient $\Delta T = 5°C$ in a 50-μm-thick sample of CCN-37 +5.9 wt% CC. A first set of results obtained with this sample is shown in Figure 6. Only droplets of diameter smaller than the sample thickness were considered here. This graph shows that the period of rotation is inversely proportional to the temperature gradient and increases when the radius R of the droplets increases. This tendency was already observed with the twisted bipolar droplets of the chromonic LC

[7]. On the other hand, if the curves $\Theta(R)$ are still linear, they no longer pass through the origin as it was observed in the chromonic LC.

We then checked if these results depend on the sample thickness. This is important because velocity variations versus thickness of almost two orders of magnitude were already observed for droplets of similar size oriented by an electric field when the thickness was changed from 10 to 70 μm [20]. With this aim, we prepared new samples with the mixture CCN-37 +5.9 wt% CC of thicknesses 20.8, 40.6, 49.2 and 70.9 μm and systematically measured the product $\Theta\Delta T$ as a function of R. Our data are reported in Figure 7 where two sets of points are visible. The first one (filled symbols) corresponds to all the droplets of diameter smaller than the sample thickness. These droplets are not confined and are expected to have a spherical shape as the banded droplets observed in the same conditions [6]. For these droplets, the rotation velocity does not depend on the sample thickness to within a factor of 2, which is within the reproducibility of the measurements. This is much less than the two orders of magnitude mentioned above and quite comparable with what was observed with the banded droplets of the usual LC when no electric field is applied [20]. The second set of points (hollow symbols) corresponds to confined droplets for which the diameter is larger than the sample thickness. These droplets are necessarily flattened in the centre and clearly slow down when $2R/d \geq 1.5$. We also note that for a given confinement $2R/d$ this effect is more important in the thick samples than in the thin ones. This is certainly due to a change of the internal texture of the droplets as we can see in photos (c) and (d) of Figure 8.
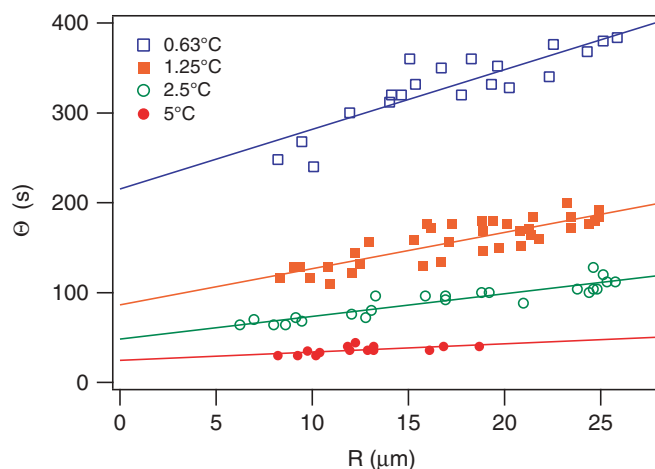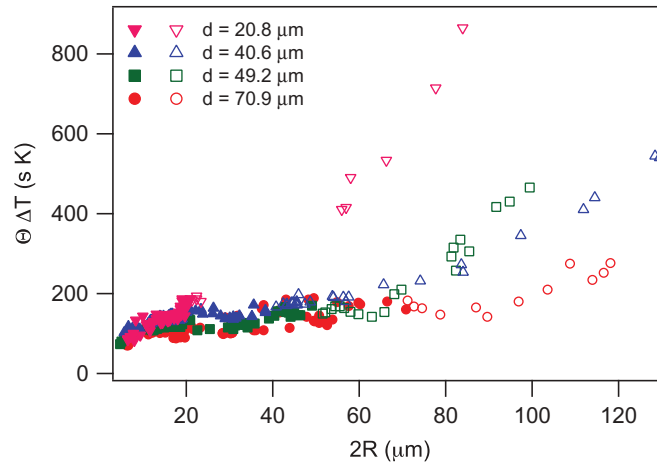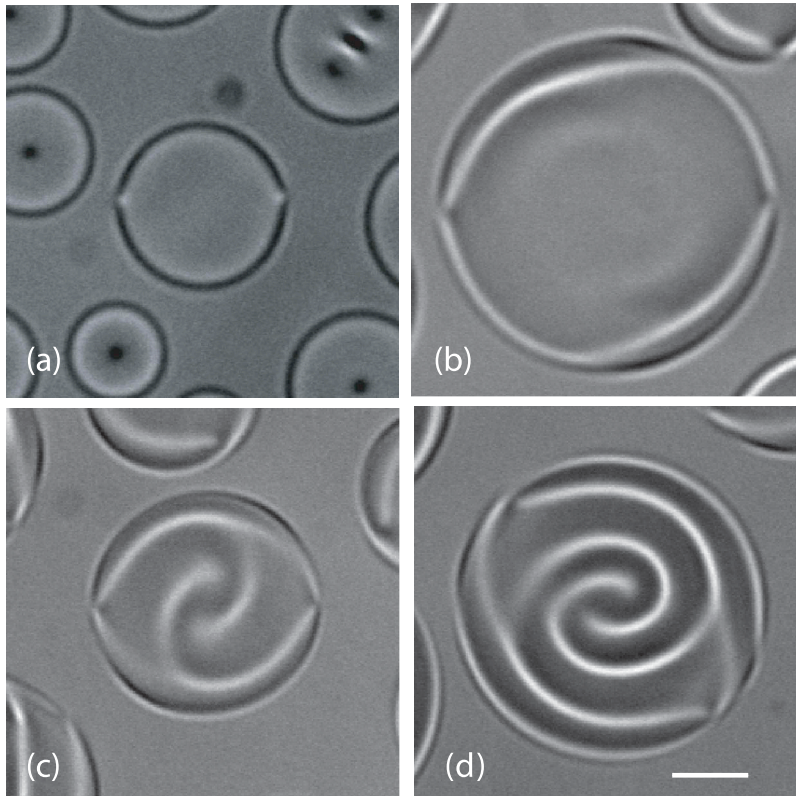

Figure 6. (Colour online) Period of rotation Θ of the droplets as a function of the radius R for different ΔT. CCN-37 +5.9% CC, $d = 50 \mu m$.
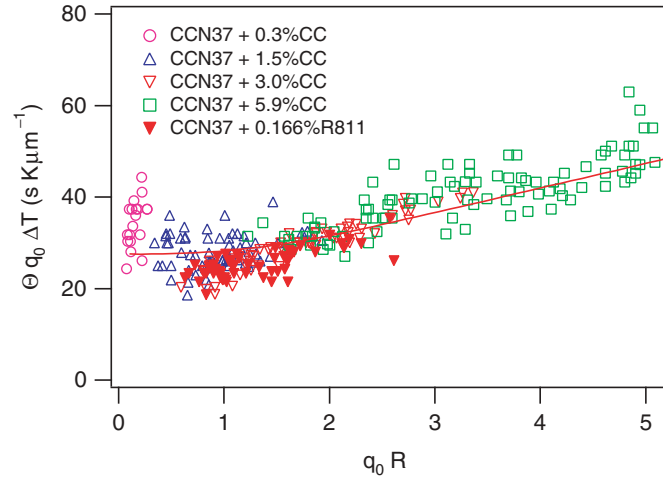
Figure 7. (Colour online) Product $\Theta\Delta T$ as a function of the droplet diameter $2R$ for different thicknesses. The filled (hollow) symbols correspond to non-confined (confined) droplets. All the samples have been prepared with the mixture CCN-37 +5.9% CC.

Figure 8. Bright field microscopy images of four confined droplets. (a) $d = 20.8\ \mu m$ and $2R/d = 2.79$; (b) $d = 40.6\ \mu m$ and $2R/d = 2.82$; (c) $d = 49.2\ \mu m$ and $2R/d = 1.66$; (c) $d = 70.9\ \mu m$ and $2R/d = 1.46$. All the samples have been prepared with the mixture CCN-37 +5.9% CC. $\Delta T = 2.5°C$ except in (d) where $\Delta T = 1.5°C$. The white bar represents 25 μm. Note the textural change in (c) and (d), although the two poles are still clearly visible.

Finally, we performed similar measurements at other concentrations of CC and with the R811. To avoid the confinement effects, only the droplets of diameter smaller than the thickness were considered. All our results obtained with 50-μm-thick samples are shown in

Figure 9, where we plotted the product $\Theta q_0 \Delta T$ as a function of the dimensionless radius $q_0 R$. In this way, all the data (including the ones obtained with the R811) collapse on the same master curve although Θ varies by two orders of magnitude, from 2 to 2000 s typically.

Figure 9. (Colour online) Product $\Theta q_0 \Delta T$ as a function of the dimensionless radius q_0R. The data have been obtained with different concentrations of CC and R811 for different ΔT. All the samples were 50 μm thick. The solid line is the best fit with the thermomechanical model.

This scaling is predicted for a given chiral molecule by the thermomechanical model proposed in Section 2. Indeed, rewriting Equation (13) in the form

$$\Theta q_0 \Delta T = 8\pi e \frac{\gamma_1}{\kappa_g/\kappa_I} \frac{L_\gamma}{(\bar{v}/q_0)L_v + \bar{\xi}L_\xi}, \qquad (18)$$

shows that $\Theta q_0 \Delta T$ is inversely proportional to $(\bar{v}/q_0)(L_v/L_\gamma) + \bar{\xi}(L_\xi/L_\gamma)$. In diluted mixtures, we found that $\bar{v}$ is proportional to the concentration of chiral molecules [17]. As q_0 is also proportional to the concentration of chiral molecules, the ratio $\bar{v}/q_0$ must be constant in all diluted mixtures prepared with the same chiral molecule. The integrals L_v, L_ξ and L_γ depend on the director field $\vec{n}_0$ and thus are functions of the droplet radius R, the spontaneous twist q_0 and the Frank elastic constants K_i ($i = 1 \ldots 4$) (including the saddle-splay constant K_4 which we define as in Ref. [1]). We assume here that the tangential anchoring is very strong at the nematic–isotropic interface, which is equivalent to assume that the anchoring extrapolation length $L_a = W_a/K_1$ is much smaller than the other lengths of the problem, namely the droplet radius R and the cholesteric pitch P. Under this assumption, the dimensionless integrals I_v, I_γ and I_ξ only depend on the dimensionless quantities $K_{i1} = K_i/K_1$ ($i = 2 \ldots 4$) and q_0R. As the ratios K_{i1} only depend on the LC chosen (here CCN-37), we conclude that for all the mixtures obtained by mixing CCN-37 with the same chiral molecule (CC or R811), the product $\Theta q_0 \Delta T$ must be an unique function of the product q_0R, whatever the concentration of chiral molecules. This is well what we

observe experimentally in the mixtures CCN-37+CC and CCN-37+R811.

On the other hand, the thermomechanical model predicts that this function of q_0R must be different with the CC and with the R811 since the ratios $\bar{v}/q_0$ measured with these two dopants below the transition temperature are very different, of the order of 11.3 fN K^{-1} for CC and 3 fN K^{-1} for R811. This is not observed. This result is the first indication that the thermomechanical model does not work because it cannot explain why the Lehmann effect does not depend on the chiral molecule chosen, but only on the value of q_0.

To further confirm this point, we fitted the data of Figure 9 with Equation 18 of the thermomechanical model by taking $\bar{v}/q_0$ and $\bar{\xi}$ as free parameters. The director field $\vec{n}_0$ was obtained numerically with a finite elements code using the deal.II library [21] by taking $K_4 = -\frac{K_1+K_2}{2}$ [22]. The ratios L_v/L_γ and L_ξ/L_γ were calculated numerically as a function of q_0R and are shown in Figure 10. The best fit of the experimental data shown in Figure 9 gives $\bar{v}/q_0 = 1.96$ pN K^{-1} and $\bar{\xi} = -1.24$ pN K^{-1}. These values are much larger, by a factor of 1000 typically, than that we measured from the rotation of the TICs (pN here, instead of fN). This difference of order of magnitude confirms that the Leslie, Akopyan and Zel'dovich thermomechanical model cannot explain the Lehmann effect. We already reached the same conclusion before by studying the banded droplets in the simplified framework of the Leslie model [20,23,24]. Our conclusion here is more general because it includes the Akopyan and Zel'dovich terms which we neglected in our previous analysis.
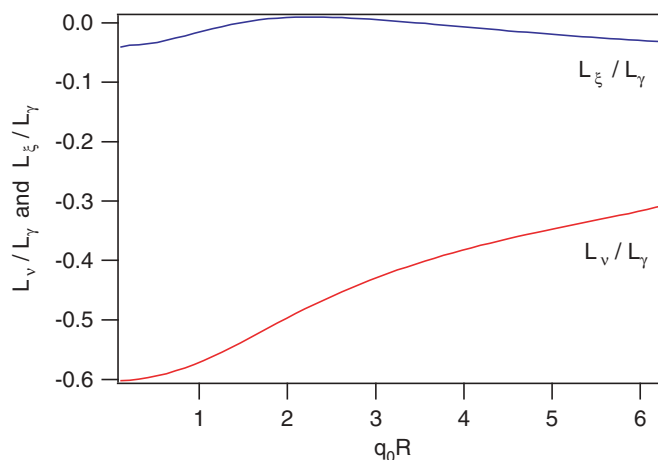
Figure 10. (Colour online) Ratios of the integrals I_ν/I_γ and I_ξ/I_γ calculated numerically as a function of the dimensionless radius q_0R.

6. Conclusion

We have shown that the Akopyan and Zel'dovich terms exist and are pertinent to explain the variations of the rotation velocity of the different TICs.

On the other hand, these terms are much too small – as the experimental Leslie coefficient $\bar{\nu}$ – to explain the rotation velocity of the twisted bipolar droplets.

These new results confirm that the Leslie paradigm, according to which the Lehmann effect is due to the thermomechanical terms, is wrong.

Another experimental evidence that the thermomechanical model cannot explain the Lehmann rotation was given while trying to observe the rotation of droplets suspended in another isotropic liquid than the isotropic phase of the LC. Indeed, according to the thermomechanical model, the droplets should rotate in any isotropic liquid. To test this idea, we prepared emulsions of the SSY chromonic nematic phase and of the CCN-37 doped with a chiral molecule in different isotropic liquids (water, hexadecane [25] or fluorinated oil [26]) but did never observe droplet rotation. This negative result works against the thermomechanical model.

In the future, it would be crucial to understand the role of the phase transition and to test the new model that we proposed in Ref. [11]. This model without the thermomechanical terms is based on the existence of an orthoradial component of the temperature gradient. This component comes from the anisotropy of the thermal conductivity of the LC and was neglected so far. The other ingredient of this model is the existence of a temperature variation of the elastic-free energy. Because of this variation, the droplet would 'surf' on a circular temperature wave that it would create itself. We are now working on this model in order to investigate whether it can explain quantitatively the Lehmann effect.

Disclosure statement

No potential conflict of interest was reported by the authors.

Note

1. For the correspondence between the coefficients, see Ref. [11].

References

[1] Oswald P, Pieranski P. Nematic and cholesteric liquid crystals: concepts and physical properties illustrated by experiments. Boca Raton: Taylor & Francis; 2005.
[2] Lehmann O. Structur, System und magnetisches Verhalten flüssiger Krystalle und deren Mischbarkeit mit festen. Ann Phys. 1900;2:649–705. DOI:10.1002/andp.19003070802
[3] Oswald P, Dequidt A. Measurement of the continuous Lehmann rotation of cholesteric droplets subjected to a temperature gradient. Phys Rev Lett. 2008;100:217802. DOI:10.1103/PhysRevLett.100.217802
[4] Oswald P. Lehmann rotation of cholesteric droplets subjected to a temperature gradient: role of the concentration of chiral molecules. Eur Phys J E. 2009;28:377–383. DOI:10.1140/epje/i2008-10431-3
[5] Yoshioka J, Ito F, Suzuki Y, et al. Director/barycentric rotation in cholesteric droplets under temperature gradient. Soft Matter. 2014;10:5869–5877. DOI:10.1039/C4SM00670D

[6] Yamamoto T, Kuroda M, Sano M. Three-dimensional analysis of thermo-mechanically rotating cholesteric liquid crystal droplets under a temperature gradient. Europhys Lett. 2015;109:46001. DOI:10.1209/0295-5075/109/46001

[7] Ignès-Mullol J, Poy G, Oswald P. Continuous rotation of achiral nematic liquid crystal droplets driven by heat flux. Phys Rev Lett. 2016;117:057801. DOI:10.1103/PhysRevLett.117.057801

[8] Zhou S, Nastishin Y, Omelchenko MM, et al. Elasticity of lyotropic chromonic liquid cystals probed by director reorientation in a magnetic field. Phys Rev Lett. 2012;109:037801. DOI:10.1103/PhysRevLett.109.037801

[9] Akopyan RS, Zel'dovich BY. Thermomechanical effects in deformed nematics. Sov Phys JETP. 1984;60:953–958.

[10] Pleiner H, Brand HR. Hydrodynamics and electrohydrodynamics of liquid crystals. In: Buka A, Kramer L, editors. Chapter 2, pattern formation in liquid crystals. New York: Springer; 1996. p. 15–67.

[11] Dequidt A, Poy G, Oswald P. Generalized drift velocity of a cholesteric texture in a temperature gradient. Soft Matter. 2016;12:7529–7538. DOI:10.1039/C6SM01359G

[12] Leslie FM. Some constitutive equations for liquid crystals. Arch Rational Mech Anal. 1968;28:265–283. DOI:10.1007/BF00251810

[13] Oswald P. Leslie thermomechanical power in diluted cholesteric liquid crystals. Europhys Lett. 2014;108:36001. Erratum: 2014;108:59001. DOI:10.1209/0295-5075/108/36001

[14] Poy G, Oswald P. Do Lehmann cholesteric droplets subjected to a temperature gradient rotate as rigid bodies. Soft Matter. 2016;12:2604–2611. DOI:10.1039/C5SM02906F

[15] Scheuble BS, Weber G, Eidenschink R. Liquid crystalline cyclohexylcarbonitriles: properties of single compounds and mixtures. Proc Eurodisplay 84-Paris. 1984;65–68.

[16] Williams RD. Two transitions in tangentially anchored nematic droplets. J Phys A: Math Gen. 1986;19:3211–3222. DOI:10.1088/0305-4470/19/16/019

[17] Oswald P. Easy axis memorization with active control of the azimuthal anchoring energy in nematic liquid crystals. Europhys Lett. 2014;107:26003. DOI:10.1209/0295-5075/107/26003

[18] Oswald P, Dequidt A. Direct measurement of the thermomechanical Lehmann coefficient in a compensated cholesteric liquid crystal. Europhys Lett. 2008;83:16005. DOI:10.1209/0295-5075/83/16005

[19] Baudry J, Brazovskaia M, Lejček L, et al. Arch-texture in cholesteric liquid crystals. Liq Cryst. 1996;21:893–901. DOI:10.1080/02678299608032907

[20] Oswald P, Poy G. Lehmann rotation of cholesteric droplets: role of the sample thickness and of the concentration of chiral molecules. Phys Rev E. 2015;91:032502. DOI:10.1103/PhysRevE.91.032502

[21] Bangerth W, Davydov D, Heister T, et al. The deal.II library, Version 8.4. J Numer Math 2016;24. DOI:10.1515/jnma-2016-1045

[22] Faetti S, Riccardi M. The phenomenological functions that characterize the surface free energy density of nematic liquid crystals: a microscopic analysis. J Physique II (France). 1995;5:1165–1191. DOI:10.1051/jp2:1995175

[23] Oswald P. Microscopic vs. macroscopic origin of the Lehmann effect in cholesteric liquid crystals. Eur Phys J E. 2012;35:10. DOI:10.1140/epje/i2012-12010-5

[24] Oswald P, Pirkl S. Lehmann rotation of the cholesteric helix in droplets oriented by an electric field. Phys Rev E. 2015;92:06512.

[25] Jeong J, Davidson ZS, Collings PJ, et al. Chiral symmetry breaking and surface faceting in chromonic liquid crystal droplets with giant elastic anisotropy. Pnas. 2013;111:1742–1747. DOI:10.1073/pnas.1315121111

[26] Ignès-Mullol J Private communication.

[27] Oswald P. Elasto- and electro-capillary instabilities of a nematic-isotropic interface: experimental results. Eur Phys J E. 2010;33:69–79. DOI:10.1140/epje/i2010-10659-2

[28] Deuling HJ. Deformation of nematic liquid crystals in an electric field. Mol Cryst Liq Cryst. 1972;19:123–131. DOI:10.1080/15421407208083858

[29] Morris SW, Palffy-Muhoray P, Balzarini DA. Measurements of the bend and splay elastic constants of octyl-cyanobiphenyl. Mol Cryst Liq Cryst. 1986;139:263–280. DOI:10.1080/00268948608080132

[30] Marinelli M, Mercuri F, Zammit U, et al. Thermal conductivity and thermal diffusivity of the cyanobiphenyl (nCB) homologous series. Phys Rev E. 1998;58:5860–5866. DOI:10.1103/PhysRevE.58.5860

[31] Pieranski P, Brochard F, Guyon E. Static and dynamic behavior of a nematic liquid crystal in a magnetic field. Part II: dynamics. J Physique (Paris). 1973;34:35–48.

[32] Martin PC, Parodi O, Pershan PJ. Unified hydrodynamic theory for crystals, liquid crystals, and normal fluids. Phys Rev A. 1972;6:2401–2420. DOI:10.1103/PhysRevA.6.2401

[33] Oswald P. Viscoelasticity of a homeotropic nematic slab. Phys Rev E. 2015;92:062508. DOI:10.1103/PhysRevE.92.062508

[34] Oswald P, Poy G. Droplet relaxation in Hele-Shaw geometry: application to the measurement of the nematic-isotropic surface tension. Phys Rev E. 2015;92:062512. DOI:10.1103/PhysRevE.92.062512

[35] Ong HL. Origin and characteristics of the optical properties of general twisted nematic liquid crystal displays. J Appl Phys. 1988;64:614–628. DOI:10.1063/1.341951

[36] Chen H, Zhu R, Zhu J, et al. A simple method to measure the twist elastic constant of a nematic liquid crystal. Liq Cryst. 2015;42:1738–1742. DOI:10.1080/02678292.2015.1070925

[37] Hanson H, Dekker AJ, van der Woude F. Analysis of the pitch in binary cholesteric liquid crystal mixtures. J Chem Phys. 1974;62:1941–1946. DOI:10.1063/1.430682

Appendix. Physical properties of the CCN-37

In this Appendix, the main physical properties of the liquid crystal CCN-37 are brought together. Several properties of this compound were already reported in Ref. [15]. Unfortunately, the authors of this paper did not pay much attention to the critical behaviour of the physical constants close to the transition to the isotropic liquid. This Appendix seeks to fill this gap with a special emphasis on the values of the constants at the transition temperature.

A.1 Dielectric constants

In order to measure the dielectric constants, we prepared 5–7-μm-thick samples of CCN-37 between two indium tin oxide (ITO) electrodes. The electrodes were treated for homeotropic (planar, resp.) anchoring by spin coating a thin layer of the polyimide compound Nissan 0626 (Nissan 0825, resp.). The layer was dried for 1 min at 80°C and then annealed at 180°C (280°C, resp.) for 30 min. The unidirectional planar anchoring was achieved by rubbing the surface with a soft felt cloth. The sample was placed into a homemade oven in which the temperature is constant and homogeneous to within ±0.01°C. The dielectric constants $\varepsilon_{\parallel}$ and $\varepsilon_{\perp}$ were obtained by measuring with a HP 4284A LCR meter the capacitance of the cell before and after filling with the LC. A 10 kHz sinusoidal voltage of amplitude 0.3–0.5 Vrms (which is well below the onset of Fréedericksz instability in homeotropic samples) was used for these measurements. Our results are shown in Figure A1, where the Merck data are also reported for comparison.

In addition, we measured the capacitance of a planar sample partly melted by imposing a vertical temperature gradient. In these conditions, the cholesteric layer was oriented for planar anchoring at the cold plate and was separated from the hot plate by a thin layer of isotropic liquid. We observed no capacitance variation as a function of the applied voltage up to 20 Vrms. The measurement was done at 1 kHz in order to minimise the heating by Joule effect in the ITO layers [27]. This is important because the thickness of the cholesteric layer must remain constant during all the measurements. The absence of capacitance variation with the applied voltage indicates that the anchoring is tangential at the nematic–isotropic interface. This was confirmed by direct observations of the sample under the microscope between crossed polarisers.
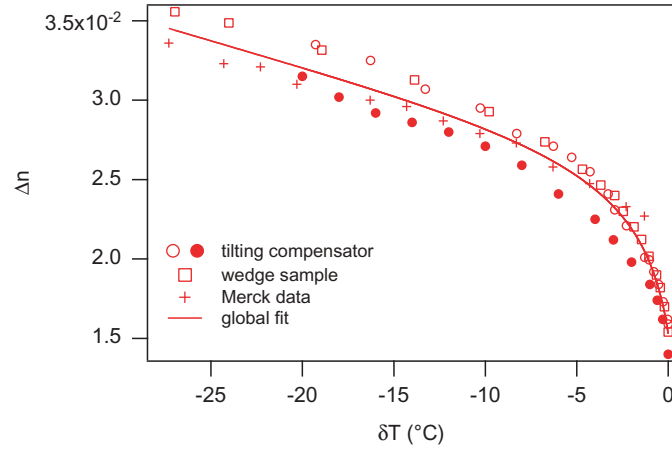
A.2 Birefringence

Two methods were used for this measurement.

First, we made a sample between two parallel glass plates treated for unidirectional planar anchoring. The sample thickness was measured to within $\pm 0.1\,\mu m$ with an USB-650 Red Tide spectrometer (Ocean Optics). Special care was taken to the parallelism between the glass plates which is here better than 10^{-4} rad. The birefringence was obtained by measuring the optical path difference between the ordinary and extraordinary rays with a $0 - 5\lambda$ tilting compensator Leitz 0989 M. All the measurements were done with green light ($\lambda = 546$ nm). In this experiment, the temperature was controlled to within ±0.01°C by placing the sample in a homemade oven regulated in temperature with the aid of a temperature controller ATNE ATSR100.

Second, we made a wedge sample by using as spacers two wires of diameters 20 and 60 μm. The two wires were parallel and spaced 2.5 cm apart. The thickness profile was determined with the spectrometer
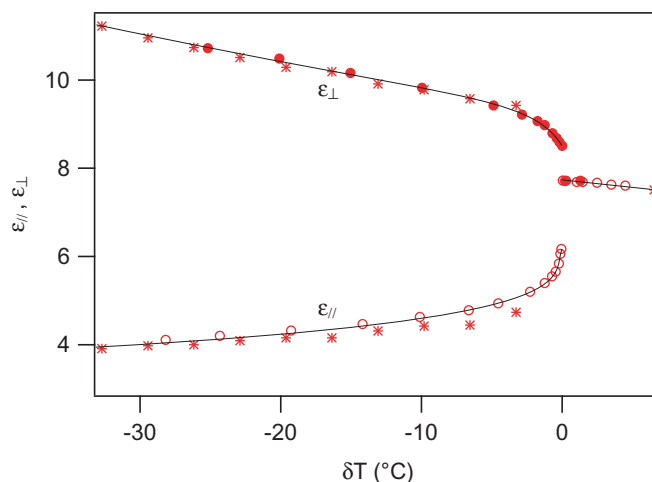
Figure A1. Dielectric constants as a function of temperature. The agreement with the Merck data (stars [15]) is good. The solid lines are guides for the eye.

Figure A2. Birefringence ($\lambda = 546\,\text{nm}$) as a function of temperature. The agreement with the Merck data (crosses [15]) is satisfactory. The solid line represents the best fit of all the data. The best fit parameters are $a = -0.032, b = 9.9 \, 10^{-5}, c = 4.9 \, 10^{-6}, d = 0.05, x_0 = 0.524$ and $n = -0.082$.

by measuring the sample thickness every 0.5 mm. The glass plates were treated for unidirectional planar anchoring and the director was parallel to the wires. The sample was placed in a special oven equipped with a long and narrow observation window allowing us to measure the transmitted intensity between crossed polarisers at 45° to the director, along a direction perpendicular to the wires. The oven was moved under the microscope with two micrometric translation stages and its temperature was regulated to within ±0.02°C thanks to a temperature controller ATNE ATSR100. The temperature inside this oven is homogeneous to within ±0.02°C. The birefringence was obtained by determining the sample thickness at the location of the black fringes where the ordinary and extraordinary rays interfere destructively. All measurements were performed with green light ($\lambda = 546$ nm).

The results obtained by these two methods are shown and compared to the Merck data in Figure A2. The solid curve is a global fit of the whole data (including the Merck data) to a law of type $a + bx + cx^2 + d/(x_0 - x)^n$. In the following, the value of birefringence calculated from this fit will be used, when necessary.

A.3 Elastic constants

The elastic constants K_3 (bend) and K_1 (splay) were obtained by measuring the capacitance of a homeotropic sample as a function of the applied voltage V (10 kHz sinusoidal voltage). A typical curve is shown in Figure A3. This curve shows the existence of a Fréedericksz instability above a critical voltage V_c of expression [1]:

$$V_c = \pi \sqrt{\frac{K_3}{-\epsilon_0 \epsilon_a}}, \qquad (A1)$$

where ϵ_0 is the vacuum permittivity and $\epsilon_a = \epsilon_\parallel - \epsilon_\perp$ is the dielectric anisotropy of the LC (here negative). The bend constant K_3 was obtained from this formula and the experimental value of the critical voltage. The constant K_1 was obtained by numerically fitting the curve $C(V)$ with the parametric equations [28]:

$$\frac{V}{V_c} = \frac{2}{\pi}\sqrt{1 + \gamma\eta}\int_0^{\pi/2}\sqrt{\frac{1 + \kappa\eta\sin^2\phi}{(1 + \gamma\eta\sin^2\phi)(1 - \eta\sin^2\phi)}}\,\mathrm{d}\phi \qquad (A2)$$

$$\frac{C}{C_\parallel} = \frac{\int_0^{\pi/2}\sqrt{\frac{(1 + \gamma\eta\sin^2\phi)(1 + \kappa\eta\sin^2\phi)}{1 - \eta\sin^2\phi}}\,\mathrm{d}\phi}{\int_0^{\pi/2}\sqrt{\frac{1 + \kappa\eta\sin^2\phi}{(1 + \gamma\eta\sin^2\phi)(1 - \eta\sin^2\phi)}}\,\mathrm{d}\phi}, \qquad (A3)$$

according to the procedure described in Ref [29]. In these equations, $C_\parallel$ is the capacitance measured below the onset of instability and $\gamma = \frac{\epsilon_\perp}{\epsilon_\parallel} - 1$ and $\kappa = \frac{K_1}{K_3} - 1$.

The constant K_2 was obtained by preparing a cholesteric mixture CCN-37+1%R811. With this mixture, the pitch is close to 11.5 μm (see Figure A8). We prepared a homeotropic sample between two ITO electrodes of thickness $d = 8$ μm, corresponding to a confinement ratio $C = d/P \approx 0.7$. At this confinement ratio, the cholesteric phase is unwound. By applying a 10 kHz AC voltage between the electrodes, the sample destabilises above a critical voltage V_c by forming periodic cholesteric fingers. The transition is second order at this value of the confinement ratio, which means that we are between the tricritical point and the triple point of the phase diagram 'homeotropic nematic–
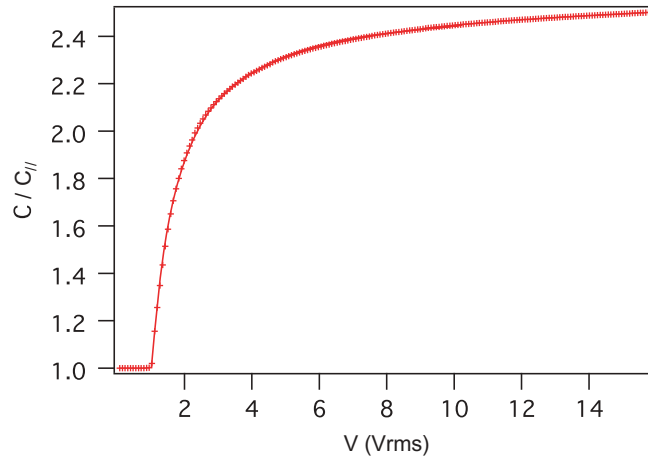
Figure A3. Normalised capacitance $C/C_{\parallel}$ as a function of the applied voltage V. $d = 7\mu m$, $\delta T = -24°C$. The solid line is the best fit obtained from the parametric equations (A2) and (A3).

cholesteric phase' observed in the parameter plane (V, C) (for details, see Ref. [1]). In this case, the critical voltage reads

$$V_c = \pi \sqrt{\frac{K_3}{-\varepsilon_0 \varepsilon_a}} \sqrt{1 - 4\frac{C^2}{K_{32}^2}}, \qquad (A4)$$

where $K_{32} = K_3/K_2$. This formula shows that the critical voltage decreases in the cholesteric phase when the confinement ratio increases. Measuring V_c in the nematic phase and in the cholesteric phase gives the ratio C/K_{32} from which K_2 can be deduced knowing C and K_3. In practice, the onset of instability was detected by locally measuring the transmitted intensity between crossed polarisers, at a place where the thickness was measured accurately with the spectrometer before filling with the LC. This technique is better than a global measurement of the cell capacitance because it is not

sensitive to an always possible lack of parallelism between the two electrodes.

Our measurements of K_1, K_2 and K_3 are shown in Figure A4.

A.4 Thermal conductivities

In order to measure the ratios of thermal conductivities $\kappa_{\parallel}^r = \kappa_{\parallel}/\kappa_g$ and $\kappa_{\perp}^r = \kappa_{\perp}/\kappa_g$ in the CCN-37, we prepared a planar sample and a mixed sample of the pure compound (for the latter, the bottom plate was treated for homeotropic anchoring and the top plate for unidirectional planar anchoring). The first one was 25.6 μm thick and the second one was 21.4 μm thick. Each sample was placed in the experimental set-up allowing to impose a temperature gradient and schematically represented in Figure A5. The temperature gradient was imposed by setting the temperatures T_t and T_b of the top and bottom
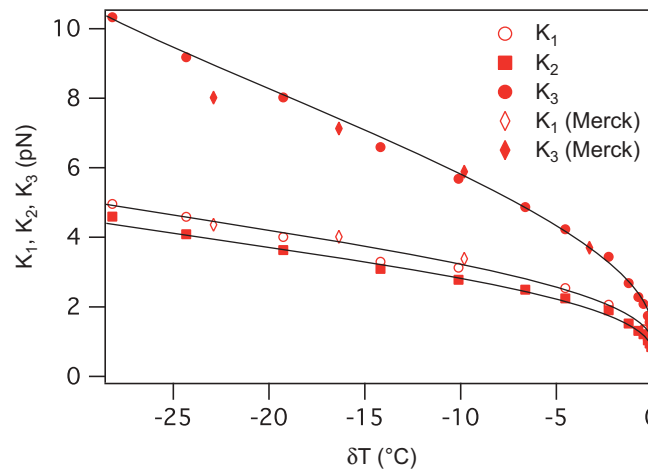
Figure A4. Splay, twist and bend constants as a function of temperature. The agreement with the Merck data (empty diamonds for K_1 and filled diamonds for K_3 [15]) is good. The solid lines are guides for the eye.
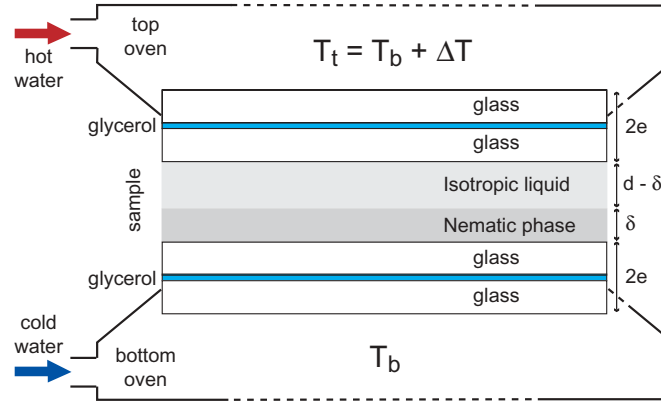
Figure A5. Schematic representation of the experimental set-up.

ovens. The temperature difference $\Delta T = T_t - T_b$ was maintained constant, equal to 40°C, during all the measurements. At the beginning, the temperatures were chosen in order that the sample was completely nematic. The experiment then consisted of measuring for each sample at which temperature $T_b^{(1)}$ the nematic phase started to melt and at which temperature $T_b^{(2)}$ the complete melting was achieved. Note that in both samples there is no discontinuity of the director orientation at the temperature $T_b^{(1)}$ when the nematic phase starts to melt because the anchoring is planar at the top surface and remains planar (tangential) at the nematic–isotropic interface. This is important to avoid hysteresis effects during the measurements of $T_b^{(1)}$, and this is the reason why we used a mixed sample instead of a homeotropic sample. In order to well detect these two temperatures, a high-resolution digital camera (Hamamatsu, model C4742-95) mounted on a Leitz Laborlux 12 Pol S polarising microscope was used. Let $\delta T_\perp$ (δT_m) be the temperature difference $T_b^{(2)} - T_b^{(1)}$ measured experimentally with the planar (mixed) sample. The ratios $\kappa_\parallel^r = \kappa_\parallel/\kappa_g$, $\kappa_\perp^r = \kappa_\perp/\kappa_g$ and $\kappa_I^r = \kappa_I/\kappa_g$ (where κ_I is the thermal conductivity of the isotropic liquid) are obtained by solving numerically the following equations:

$$\delta T_\perp = \frac{d_\perp \left[2e(\kappa_I^r + \kappa_\perp^r) + d_\perp\right]}{(4e\kappa_I^r + d_\perp)(4e\kappa_\perp + d_\perp)} \Delta T \tag{A5}$$

$$\delta T_m = \frac{d_m \left[2e(\kappa_I^r + \sqrt{\kappa_\parallel^r \kappa_\perp^r}) + d_m\right]}{(4e\kappa_I^r + d_m)\left(4e\sqrt{\kappa_\parallel^r \kappa_\perp^r} + d_m\right)} \Delta T \tag{A6}$$

$$\kappa_I^r = \frac{1}{3}\left(\kappa_\parallel^r + 2\kappa_\perp^r\right), \tag{A7}$$

where $d_\perp$ (d_m) is the thickness of the planar (mixed) sample. These equations were obtained (1) by expressing that the heat flux across the four glass plates (each

of thickness e), the layer of nematic phase (of thickness δ, see Figure A5) and the layer of isotropic liquid (of thickness $d - \delta$) is conserved in the stationary regime and (2) by writing that $\delta = d$ at $T_b = T_b^{(1)}$ and $\delta = 0$ at $T_b = T_b^{(2)}$. Note that in this calculation we neglected the influence of the two very thin layers of glycerol used to ensure a good thermal contact between the glass plates of the sample and of the ovens. In addition, we assumed that the LC was pure. This is almost the case for our CCN-37 LC for which we measured a coexistence range of the order of 0.02°C at the melting temperature (which is negligible with respect to the measured δT). Finally, we assumed that in the mixed sample the angle between the director and the normal to the plates changes linearly from 0 to $\pi/2$ as a function of z inside the nematic layer. This is an excellent approximation. In this limit, the nematic layer behaves exactly like a layer of thermal conductivity $\sqrt{\kappa_\parallel \kappa_\perp}$.

Experimentally, we measured $\delta T_m = 1.31 \pm 0.02$°C for $d_\parallel = 21.45\ \mu$m and $\delta T_\perp = 1.72 \pm 0.02$°C for $d_\perp = 25.6\ \mu$m. By taking $e = 1$ mm, the calculation gives $\frac{\kappa_\parallel}{\kappa_g} = 0.200 \pm 0.015$ and $\frac{\kappa_\perp}{\kappa_g} = 0.132 \pm 0.004$ and $\frac{\kappa_I}{\kappa_g} = 0.155 \pm 0.002$.

As expected, these values are very close to typical values measured in cyanobiphenyls [30].
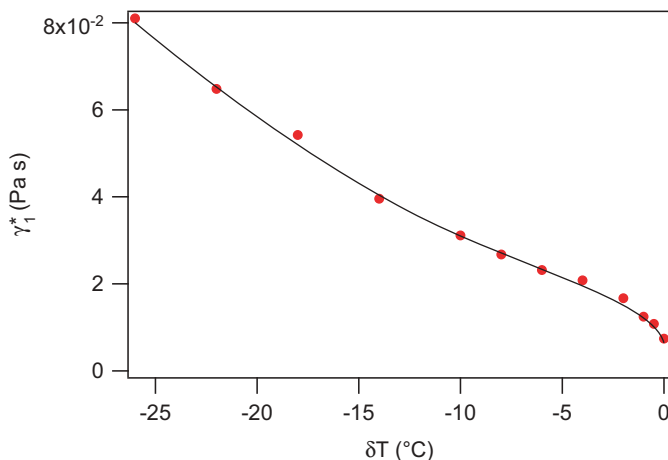
A.5 Rotational viscosity

The rotational viscosity of the CCN-37 LC was obtained by measuring the relaxation dynamics of a homeotropic sample of thickness $d = 70.5\ \mu$m initially destabilised by the application of a 1 kHz AC voltage V slightly larger than the critical voltage V_c (here, $V = 1.05 V_c$). In practice, the sample is destabilised under a 1 T magnetic field parallel to the electrodes in order that the director tilts everywhere in the same plane (here perpendicular to the magnetic field since

the magnetic anisotropy of the CCN-37 is negative [15]). A Halbach magnet is used to produce the magnetic field. The sample is then removed from the magnet and the voltage is switched off. In this way, the sample relaxes to its initial homeotropic configuration. The relaxation time τ is obtained by measuring the transmitted intensity between crossed polarisers at 45° to the distortion plane. More precisely, the intensity is fitted to the exponential law $I = I_0 \exp(-2t/\tau)$ where $\tau = \gamma_1^\star d^2/K_3\pi^2$. Note that the rotational viscosity measured in this way is an effective viscosity (slightly smaller than γ_1) that takes into account the backflow effect [31]. Our results for the effective viscosity $\gamma_1^\star$ are shown in Figure A6. In this paper, we are especially interested by the value of γ_1 at the phase transition temperature. At this temperature, the backflow correction is expected to be small and can be calculated analytically in this limit. A straightforward calculation shows that $\frac{\gamma_1^\star}{\gamma_1} = 1 - \left(1 - \frac{8}{\pi^2}\right)\frac{\eta_c - \nu_3}{\eta_c}$ where η_c is the third Miesowicz viscosity [1] and ν_3 a smaller viscosity first introduced by Martin, Parodi, and Pershan [32]. Recently, we have shown how to measure these two viscosities with a piezoelectric rheometer [33]. By using this technique, we measured $\eta_c = 0.039$Pa s [34] and $\nu_3 = 0.026$ Pa s at the transition temperature in the CCN-37. With these values, we calculate at the transition temperature $\gamma_1 = 0.0069$ Pa s knowing that $\gamma_1^\star = 0.0074$ Pa s. As we can see, the backflow effect is small (of the order of 6%), justifying a posteriori the validity of the formula given above.

A.6 HTP of R811 and CC

Let C be the concentration by weight of chiral dopant added to the CCN-37 LC. The HTP is defined to be the ratio $1/(PC)$, where P is the cholesteric pitch. The cholesteric pitch (or the equilibrium twist $q_0 = 2\pi/P$) was measured by using the Cano-wedge method [1]. In practice, the cholesteric phase was placed between two glass plates treated for unidirectional planar anchoring (rubbed polyimide) and making a small angle. The rubbing direction was chosen parallel to the two nickel wires of diameters 15 and 68 µm used as spacers and placed 25 mm apart. The thickness profile was determined by measuring the local thickness every 0.5 mm with the spectrometer. The sample temperature was controlled with the same homemade oven as the one used to measure the birefringence with the wedge sample. By noting the position of the κ-disclination lines, the absolute value of the pitch was determined.

In order to determine the sign of the pitch, the cholesteric mixture was placed between two parallel glass plates. The bottom glass plate was treated for unidirectional planar anchoring (rubbed polyimide) and the top glass plate for tangential sliding anchoring (polymercaptan). Once inside the oven, the sample was observed under the polarising microscope with green light ($\lambda = 546$nm). The measurement consisted of recording the transmitted intensity I_{tr} as a function of the angle ϕ between the analyser and the polariser while maintaining the polariser parallel to the rubbing direction. A typical curve is shown in Figure A7. This curve passes through a

Figure A6. Effective rotational viscosity of the CCN-37 LC as a function of temperature. The solid line is a guide for the eye.
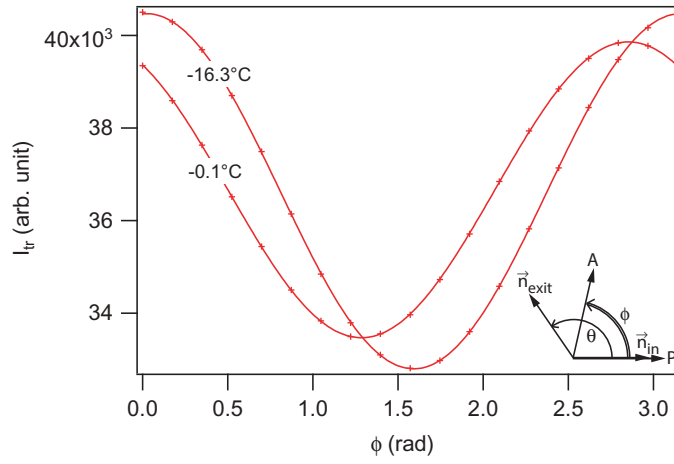
Figure A7. Two curves of transmitted intensity I_{tr} measured in green light ($\lambda = 546$nm) at two different δT as a function of angle ϕ between the analyser and the polariser. Mixture CCN-37+3% CC, $d = 7.32$ μm. The best fit to a sine function (solid line) gives $\phi_{min} = 1.285$ rad at $\delta T = -0.1°$C and $\phi_{min} = 1.592$ rad at $\delta T = -16.3°$C. The latter value of ϕ_{min} is close to $\pi/2$, which indicates the proximity of a compensation point. Inset: definition of the angles θ and ϕ.

minimum at $\phi = \phi_{min}$ obtained from a fit to a sine function. An important point to note here is that the value of ϕ_{min} measured at a given temperature δT was independent of the thermal history of the sample. This shows once again that the polymercaptan treatment is perfectly sliding throughout the duration of the experiment. The value (and the sign) of the pitch was then calculated by using the Ong formula [35]:

$$I_{tr}(\phi) = \cos^2(\theta - \phi)$$
$$- \frac{\cos[2(\theta - \phi)]\sin^2[\theta\sqrt{1 + u^2}]}{1 + u^2}$$
$$+ \frac{\sin[2(\theta - \phi)]\sin[2\theta\sqrt{1 + u^2}]}{2\sqrt{1 + u^2}} \qquad (A8)$$

where $\theta = q_0 d = \frac{2\pi d}{P}$ is the angle of rotation of the director across the sample thickness and $u = \frac{\pi d \Delta n}{\theta \lambda}$.

More exactly, θ was calculated numerically with Mathematica by assuming that the function $I_{tr}(\phi)$ passes through a minimum at $\phi = \phi_{min}$.

The result of our measurements with these two methods are shown in Figure A8 for the mixture CCN-37 +0.166% R811 and the mixture CCN-37+3% CC. In the case of the R811 dopant, we observe, as expected, that the HTP is positive (right-handed cholesteric) and changes very little with the temperature: HTP $\approx 9\mu m^{-1}$ which is slightly smaller than in usual LCs where typical values between 9.5 and 13 μm^{-1} are found [36]. On the other hand, the behaviour of the mixture CCN-37+3% CC is very surprising for two reasons: first, because the cholesteric phase is right-handed at the transition temperature, and second, because this mixture has a compensation point about 16° below the transition temperature. Indeed, in usual LCs such as biphenyls or MBBA, the
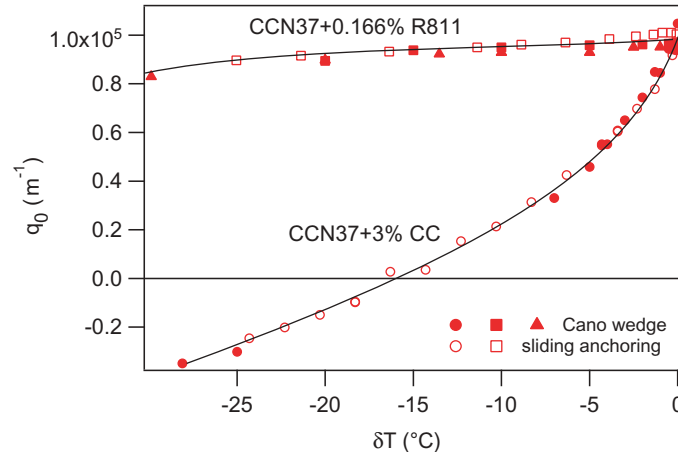
Figure A8. Equilibrium twist as a function of temperature measured with the two cholesteric mixtures CCN-37+0.166% R811 and CCN-37+3% CC. Each symbol corresponds to a different sample. The solid curves are guides for the eye.
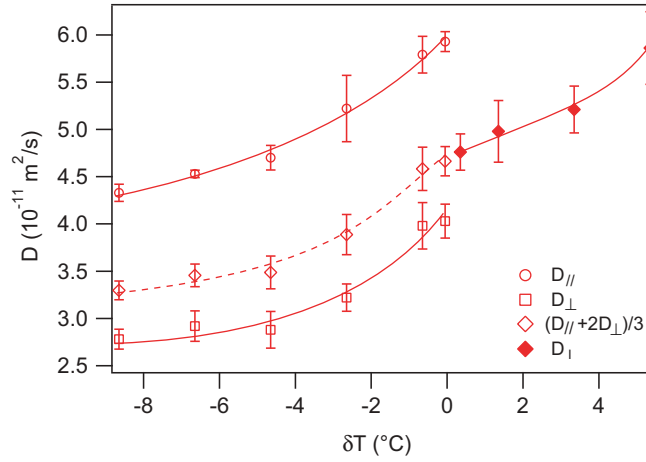
Figure A9. Diffusion coefficients of the fluorescent dye NBD C6-ceramide in the nematic and isotropic phases of the CCN-37 LC measured by FRAP. The solid and dashed lines are guides for the eye.

CC gives left-handed cholesterics at low concentration [13] and a compensation point is only observed at large concentrations of CC (40% or more) [18,23,37]. Another point to emphasise is that the mixture CCN-37+3% CC is a rare example (to our knowledge) of compensated mixture with a negative dielectric anisotropy.

A.7 Diffusion coefficients of the fluorescent dye

We measured by FRAP the diffusion coefficients of the fluorescent dye NBD C6-ceramide in the nematic and isotropic phases of the CCN-37 LC. For this experiment, we prepared a 21-μm-thick sample of the mixture CCN-37+0.05wt% NBD C6-ceramide. The two glass plates were treated for unidirectional planar anchoring along the direction x (rubbing direction). The fluorescence signal was measured as in Ref. [14] and was fitted by a Gaussian function of type $s(t) + \Delta s(t) \exp\left[-\frac{x^2}{2\sigma_\parallel^2} - \frac{y^2}{2\sigma_\perp^2}\right]$ in the nematic phase and of type $s(t) + \Delta s(t) \exp\left[-\frac{x^2+y^2}{2\sigma_I^2}\right]$ in the isotropic liquid. The diffusion coefficients are deduced from a fit of $\sigma^2(t) - \sigma^2(0)$ with a straight line of slope $2D$. Our results are shown in Figure A9. From these data, we calculate at the transition temperature $(D_\parallel + 2D_\perp)/3 \approx 4.7 \, 10^{-11}$ m^2/s, which is indeed very close to $D_I \approx 4.8 \, 10^{-11}$ m^2/s.